ENVIRONMENTAL ENGINEERING SCIENCE
Volume 27, Number 3, 2010

DOI: 10.1089/ees.2009.0359

Integrated Modeling System for Water Resources Management of Tarim River Basin

Yue Huang,[1] Xi Chen,[2] Yongping Li,[1,*] Patrick Willems,[3] and Tie Liu[3]

[1]College of Urban and Environmental Sciences, Peking University, Beijing, People's Republic of China.
[2]Xinjiang Institute of Ecology and Geography, Chinese Academy of Sciences, Urumqi, People's Republic of China.
[3]Department of Civil Engineering, Katholieke University Leuven, Leuven, Belgium.

Received: October 28, 2009 *Accepted in revised form: January 4, 2010*

Abstract

An integrated modeling system has been developed for water resources management of the Tarim River Basin, China. The system coupled remote sensing (RS)/geography information system (GIS) technique with distributed hydrological model to simulate the rainfall runoff, snow melting, and evapotranspiration process of the hydrological cycle. A case study was carried out in the Kaidu watershed. RS/GIS technique was used for effectively accessing, processing, and managing spatial data, such as land use, vegetative cover, soil, topography, precipitation, and evapotranspiration. The model was calibrated and validated against observed discharge for two hydrological stations during the period 1998–2001, and it generally performed well for Nash-Sutcliffe coefficient, water balance coefficient, and correlation coefficient. The Nash-Sutcliffe coefficient was approximately over 0.7 and the water balance error was lower than $\pm 5\%$, indicating reasonable prediction accuracy. A comparison between the conventional and RS-based hydrological models was conducted. Although the two models exhibit similar performances on runoff and snow melt simulation, the RS-based hydrological model had better performance in the simulation of actual evapotranspiration. Modeling results provide useful decision support for water resources management.

Key words: distributed hydrological model; remote sensing; Tarim River Basin; water resources management

Introduction

Currently, one-third of the world's population is living in countries and regions of water resources limitation (Bates, *et al.*, 2008). Because of limited water availability imposing strong restrictions on natural and human systems, the management of water resources has become an increasingly pressing issue in semiarid and arid regions. For example, the Northwest of China is a typical arid region that is characterized by low and irregular rainfall, high temperatures and evaporation, and notable drought periods. In this region, water shortage has become an increasingly serious problem, where demand outstrips water resources availability because of chronic severe shortages. The surface water and ground water in this region only account for 3.3% and 5.5%, respectively, of the national total, whereas the area occupies 24.5% of Chinese total landmass (Ma, 2005). Generally, when the demand of water has reached the limits of what the natural system can provide, water shortage can become a major obstacle to social and economic development for one region (Bronster *et al*., 2000; Li *et al*., 2006). Therefore, these issues have forced planners to contemplate and propose ever more comprehensive, complex, and ambitious plans for water resources systems in the semiarid and arid regions (Li *et al*., 2008).

Hydrologic model was a useful tool for water resources management (Sahoo *et al*., 2006). Previously, many lumped hydrologic models were developed to investigate watershed hydrology. For example, Crawford and Linsey (1966) advanced the Stanford watershed model for Los Trancos Creek, which is a crude water balance model without considering enough structural elements to follow process adequately. Burnash *et al*. (1973) developed the Sacramento soil moisture accounting model for operational river forecasting. Jakeman *et al*. (1990) proposed a hybrid conceptual-metric model, IHACRES, for rainfall-runoff simulation of two small upland catchments. With a low data requirement, these lumped catchment models could reflect runoff dynamics and water balance in water resource management systems. However, the lumped models assumed the study watershed as a spatially homogeneous region, and the spatial heterogeneity of the climate variable and land surface was not considered (Bronster *et al*., 2000).

Consequently, several distributed and semidistributed hydrological models were developed in response to the

*Corresponding author: College of Urban and Environmental Sciences, Peking University, Beijing 100871, People's Republic of China. *Phone:* 86-10-62756137; *Fax:* 86-10-62756137; *E-mail:* yongping.li@urban.pku.edu.cn

aforementioned challenges (Apul *et al*., 2005). For example, Beven (1979) developed TOPMODEL to simulate small upland catchments in United Kingdom, and reasonable results with a minimum calibration value for modeling parameters were obtained. Grayson *et al*. (1992) developed a simple distributed hydrological model (i.e., THALES) and applied it to two catchments in Australia and the United States, each with different dominant hydrological responses. Refsgaard (1997) integrated MIKE SHE, MIKE 11, MIKE 21, and DAISY to study the environmental assessment in connection with the Gabcikovo hydropower scheme. Sahoo *et al*. (2006) used the physically distributed hydrological modeling system (MIKE SHE) to study the watershed response to storm events within the Manoa-Palolo stream system on the island of Oahu, Hawaii. The primary advantage of the distributed hydrological models was enabled to reflect the spatial variations for characteristics of watershed (e.g., rainfall, topography, soil type, and land use) (Refsgaard, 1997). However, higher data requirement became a main obstacle on extensively applying these models to practical problems.

As a result, many researchers focused on using remote sensing (RS) technique to supply relevant spatial data and parameters at the appropriate scale for distributed hydrological models (Xu *et al*., 2007; Stisen *et al*., 2008). RS data with high resolution in both space and time were available in many areas where data are typically unavailable. A number of researchers used the RS technique to obtain the land surface parameters. For example, Biftu and Gan (2001) developed a semidistributed hydrological model (DPHM-RS), where RS technique was used for parameterization of the land surface. McMichael *et al*. (2006) used MIKE SHE model to estimate monthly stream flow in a semiarid shrub land catchment in central California, where remote-sensed leaf area index (LAI) data were used for describing the characters of vegetation. Besides, a few researchers used RS technique to obtain the climatic parameters. For example, Andersen *et al*. (2001) employed MIKE SHE model for simulating the runoff in the Senegal River Basin, where remotely sensed precipitation and LAI data were used. Grimes and Diop (2003) developed a hydrological model for the Qualia catchment, where remotely sensed rainfall was used as modeling input. Stisen *et al*. (2008) used the MIKE SHE hydrological model for the Senegal River Basin by utilizing RS data to estimate precipitation, potential evapotranspiration (PET), and LAI. However, the data based on satellite products without enough accuracy may lead to uncertainties and biases (Stisen *et al*., 2008). Therefore, to more effectively reflect the real-world system, it is desired to integrate RS/geography information system (GIS) technique and distributed hydrological model into a general framework.

Tarim River is located in northwest of China and is the longest inland river all over the country. This basin is a typical water-shortage area, with characteristics of low rainfall, high temperature, and high evaporation. In the past decades, water shortage has become increasingly serious in this basin because of population growth and economic development. Previously, most of the studies for the hydrological process of this basin were based on statistic methods (Wu, 2003; Deng, 2006; Xu *et al*., 2007; Zhang *et al*., 2004). For example, Zhang (2006) used NAM model to simulate the rainfall-runoff and snow melting flows in the Kaidu watershed, and the results showed a low accuracy for using limited observation data. Ouyang *et al*. (2007) constructed four hydrologic forecast approaches to simulate daily runoff of two big branches of the Aksu Watershed in the Tarim region. Zhao *et al*. (2009) developed a dissipative hydrological model to study moisture transformation in the Hotan catchment. However, because of the lack of enough data required, few researchers paid attention on managing this watershed through RS/GIS technique and physical distributed hydrological model.

Therefore, the objective of this study was to develop an integrated modeling system through coupling RS/GIS technique with distributed hydrological model for water resources management of the Tarim River Basin. In the integrated modeling system, RS/GIS can be used for effectively accessing, processing, and managing spatial data, such as land use, vegetative cover, soil, topography, precipitation, and evapotranspiration of concerned watershed; MIKE SHE model will be used for simulating water movement in the entire land phase of the hydrological cycle. The results obtained will be used for helping planners to establish effective water exploitation and allocation policies and thus improve the local ecosystem sustainability.

Methodology

Distributed hydrological model

The MIKE SHE model is a physical distributed hydrological modeling system covering the entire land phase of the hydrological cycle (Abbott *et al*., 1986). The model consists of five modules: overland flow, evapotranspiration, unsaturated flow, saturated flow, and channel flow modules (DHI, 1999). The overland flow module is based on the dynamic solution of the two-dimensional Saint-Venant equations. The diffusive wave approximation is used to calculate the surface flow in x and y directions. Rectangular Cartesian (x, y) coordinates is used in the horizontal plane. Thus, we have

$$\frac{\partial h}{\partial t} + \frac{\partial}{\partial x}uh + \frac{\partial}{\partial y}vh = i \tag{1}$$

$$\begin{cases} S_{\mathrm{f}x} = S_{\mathrm{o}x} - \frac{\partial h}{\partial x} \\ S_{\mathrm{f}y} = S_{\mathrm{o}y} - \frac{\partial h}{\partial y} \end{cases} \tag{2}$$

$$\begin{cases} uh = K_x\left(-\frac{\partial h}{\partial x}\right)^{1/2} h^{5/3} \\ vh = K_y\left(-\frac{\partial h}{\partial y}\right)^{1/2} h^{5/3} \end{cases} \tag{3}$$

where $h(x, y)$ is the flow depth above the ground surface; t is time (s); $u(x, y)$ and $v(x, y)$ are the flow velocities in x and y directions; $i(x, y)$ is the net input into overland flow; S_{f} is the friction slopes in x and y directions; S_{o} is the slope of the ground surface; K_x and K_y are Strickler coefficients in x and y directions; uh and vh represent discharge per unit length along the cell boundary in the x and y directions, respectively.

In the MIKE SHE model, the method proposed by Kristensen and Jensen (1975) was used for calculating actual evapotranspiration (AET), based on a number of parameters such as PET, LAI, and root depth for each vegetation type. The evapotranspiration section was divided into three subsections (i.e., the interception storage capacity, the transpiration from

the vegetation, and the soil evaporation). The size of the interception storage capacity (E_{can}) depends on the vegetation type and its stage of development, which is characterized by LAI. Thus, we have

$$E_{can} = \min(I_{max}, P_{ET}\Delta T) \tag{4}$$

$$I_{max} = C_{int} \times \mathrm{LAI} \tag{5}$$

where E_{can} is the canopy evaporation [LT^{-1}]; P_{ET} is the PET rate [LT^{-1}]; ΔT is the time step length for the simulation; C_{int} is an interception coefficient; LAI is leaf area index. The coefficient (C_{int}) defines the interception storage capacity of the vegetation.

The transpiration from the vegetation depends on the density of the crop green material (i.e., LAI), the soil moisture content in the root zone, and the root density. Thus, we have

$$E_{at} = f_1(\mathrm{LAI}) \cdot f_2(\theta) \cdot RDF \cdot P_{ET} \tag{6}$$

$$f_1(\mathrm{LAI}) = C_2 + C_1\mathrm{LAI} \tag{7}$$

$$f_2\theta = 1 - \left(\frac{\theta_{FC} - \theta}{\theta_{FC} - \theta_W}\right)^{\frac{C_3}{E_P}} \tag{8}$$

where E_{at} is the actual transpiration, f_1(LAI) is a function based on the LAI, $f_2(\theta)$ is a function based on the soil moisture content in the root zone; RDF is a root distribution function; θ_{FC} is the volumetric moisture content at field capacity; θ_W is the volumetric moisture content at the wilting point; θ is the actual volumetric moisture content;C_1 and C_2 are empirical parameters [-]; C_3 is an empirical parameter [LT^{-1}].

Soil evaporation (E_S) can occur from the upper part of the unsaturated zone and consists of a basic amount of evaporation, plus additional evaporation from excess soil water as the soil saturation reaches field capacity. The value for E_S can be calculated by the following formula:

$$E_S = P_{ET} \cdot f_3(\theta) + (P_{ET} - E_{at} - P_{ET} \cdot f_3(\theta) \cdot f_4(\theta) \cdot (1 - f_1(\mathrm{LAI}))) \tag{9}$$

where P_{ET} is the PET; E_{at} is the actual transpiration; f_1(LAI) is a function based on the LAI; $f_3(\theta)$ and $f_4(\theta)$ are the functions based on the actual volumetric moisture content.

$$f_3(\theta) = \begin{cases} C_2 & \text{for } \theta \geq \theta_W \\ C_2\dfrac{\theta}{\theta_W} & \text{for } \theta_r \leq \theta \leq \theta_W \\ 0 & \text{for } \theta \leq \theta_r \end{cases} \tag{10}$$

$$f_4(\theta) = \begin{cases} \dfrac{\theta - \dfrac{\theta_W + \theta_{FC}}{2}}{\theta_{FC} - \dfrac{\theta_W + \theta_{FC}}{2}} & \text{for } \theta \geq \dfrac{\theta_W + \theta_{FC}}{2} \\ 0 & \text{for } \theta < \dfrac{\theta_W + \theta_{FC}}{2} \end{cases} \tag{11}$$

The total AET is defined as the sum of E_{can}, E_{at}, and E_S and has an upper limit corresponding to the PET.

The unsaturated flow is considered as a vertical one-dimensional process. In the Richards equation, the driving force for transport of water in the unsaturated zone is the gradient of the hydraulic head (h), which includes a gravitational component (z) and a pressure component (ψ). Thus, we have

$$h = z + \psi \tag{12}$$

$$C\frac{\partial\psi}{\partial t} = \frac{\partial}{\partial z}\left(K(\theta)\frac{\partial\psi}{\partial z}\right) + \frac{\partial K(\theta)}{\partial z} - S \tag{13}$$

where h is the gradient of the hydraulic head, which includes a gravitational component (z) and a pressure component (ψ); θ is the volumetric soil moisture; S is the root extraction sink term; $K(\theta)$ is the hydraulic conductivity function; $\psi(\theta)$ is the soil moisture retention curve.

The saturated flow that is allowed for a fully three-dimensional (3D) way is described by the Darcy equation and solved by the iterative implicit finite difference technique. 3D finite difference method is used to simulate the 3D saturated flow in saturated porous media. Thus, we have

$$\frac{\partial}{\partial x}\left(K_{xx}\frac{\partial h}{\partial x}\right) + \frac{\partial}{\partial y}\left(K_{yy}\frac{\partial h}{\partial y}\right) + \frac{\partial}{\partial z}\left(K_{zz}\frac{\partial h}{\partial z}\right) - Q = S\frac{\partial h}{\partial t} \tag{14}$$

where K_{xx}, K_{yy}, and K_{zz} are the hydraulic conductivity along the x, y, and z directions. They are assumed to be parallel to the principle axes of hydraulic conductivity tensor. The h is the hydraulic head, Q represents the source/sink terms, and S is the specific storage coefficient.

The channel flow is calculated by the one-dimensional simulation using the full dynamic Saint Venant equations. The coupling between MIKE SHE and MIKE 11 is made via river links. The river links can be considered as medium between two computational components.

$$\frac{\partial h}{\partial t} + \frac{\partial}{\partial x}uh = i \tag{15}$$

$$S_{fx} = S_{ox} - \frac{\partial h}{\partial x} \tag{16}$$

where h is the flow depth above the ground surface, t is time (s), u is the flow velocity, i is the net input into overland flow, S_f is the friction slopes, S_o is the slope of the ground surface, and uh represents discharge.

RS technique

In this study, RS technique is used for estimating several modeling inputs such as precipitation, PET, and LAI. Rainfall is discontinuous in space and time. It is difficult to obtain rainfall distribution in detail if only few rain gauges are used. Fengyun (FY_2C) meteorological satellite provides hourly observations over the whole territory of the P.R. China. The rainfall estimation is carried out by the method developed by the Chinese National Satellite Meteorological Centre. The method is based on satellite-derived cold cloud duration. The relationship between the cloud top temperature gradient and rainfall rate was used to estimate rainfalls (as shown in Figure 1). Figure 2 shows a flow diagram of the technique. To accommodate for the relationship presented in Fig. 1, clouds are subdivided according to cloud top temperature. In this

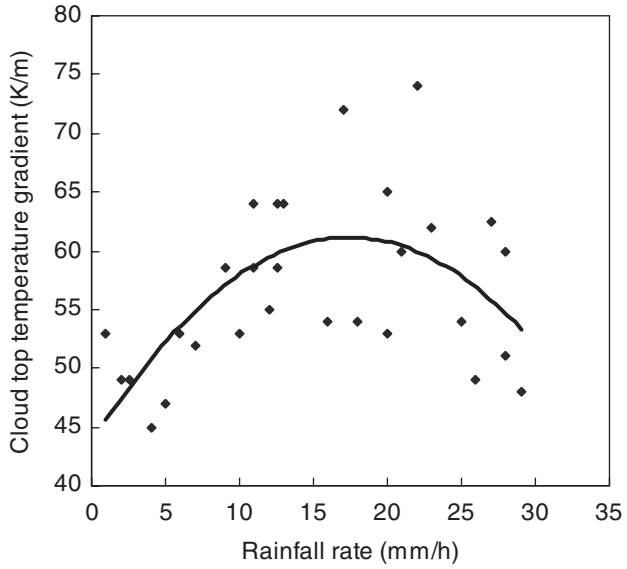

FIG. 1. Relationship between cloud top temperature gradient and rainfall rate.

study, the FY_2C rainfall products are calibrated using daily observations of rainfall from two gauges within the Kaidu watershed for the year 2005.

The estimation of PET is based on the energy balance and the SEBAL model (Bastiaanssen *et al.*, 1998; Su, 2002). The energy fluxes can be determined as instantaneous values at the time of the Aqua/MODIS satellite overpass. Thus, we have

$$R_n - G_0 - H - \lambda E = 0 \tag{17}$$

$$\Lambda = \frac{\lambda E}{H + \lambda E} \approx \frac{\mathrm{LST}_H - \mathrm{LST}_0}{\mathrm{LST}_H - \mathrm{LST}_{\lambda E}} \approx \frac{a_H\, a_0\, b_H - \mathrm{LST}_0}{(a_H - a_{\lambda E})a_0 + (b_H - b_{\lambda E})} \tag{18}$$

where R_n is net radiation (net short wave and net long wave) [W m^{-2}], G_0 is the soil heat flux [W m^{-2}], H is the sensible heat flux [W m^{-2}], λE is the latent heat flux [W m^{-2}], Λ is the ratio of the amount of latent heat; LST_H is the land surface temperature for dry pixels [K], $\mathrm{LST}_{\lambda E}$ is the land surface temperature for wet pixels [K], LST is the land surface temperature for the considered pixel [K], a_0 is the surface albedo, a_H, $a_{\lambda E}$ are the slopes of the line of the high and low temperatures, respectively, as a function of surface albedo [K], and b_H, $b_{\lambda E}$ are

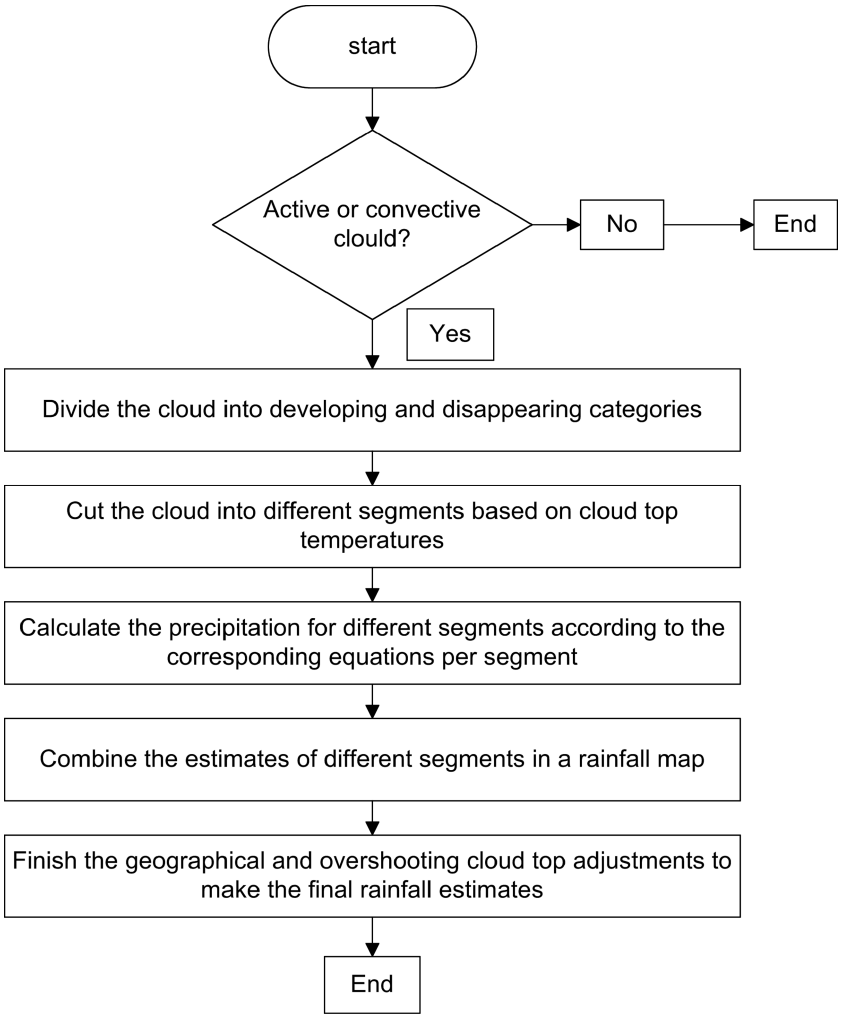

FIG. 2. Flow diagram to estimate hourly rainfall, as developed by the National Satellite Meteorological Centre.

the intercepts of the line of the high and low temperatures, respectively, as a function of surface albedo [K]. Then, the daily ET can be calculated using the following formula:

$$\mathrm{ET} = \Lambda \frac{R_{\mathrm{nd}}}{28.588} \tag{19}$$

where ET is the daily evapotranspiration [mm/day], Λ is the evaporative fraction, R_{nd} is the daily net radiation [W m^{-2}]. The RS-based method has been tested against measurements from local sites within the Xinjiang, China. Then the verified PET data are applied to the Kaidu watershed.

LAI is a widely used biophysical parameter that describes the abundance of vegetation. The RS-based data could help improve the spatial and temporal resolution of LAI inputs, which is also the basis of estimating the root depth and crop coefficient (K_c). It cannot be detected directly from satellite RS, but numerous studies have shown the existence of a nonlinear relation between LAI and the commonly used normalized difference vegetation index (NDVI). The NDVI is calculated by exploiting the characteristics of the spectral signature for green vegetation. Thus, we have

$$\mathrm{NDVI} = \frac{\mathrm{NIR} - \mathrm{RED}}{\mathrm{NIR} + \mathrm{RED}} \tag{20}$$

where RED is the reflectance in the red spectrum, and NIR is the near infrared spectrum. The conversion from NDVI to LAI is not straight forward because bidirectional reflectance distribution functions should be taken into account. A sophisticated LAI retrieval is included in the MODIS LAI/FPAR 8-day L4 global 1 km products, which are downloaded for hydrological modeling in this study.

Development of an Integrated Modeling System for Tarim River Basin

Overview of study system

The Tarim River is formed by the union of Aksu, Hotan, and Yarkant rivers at the western, and flows east along the northern edge of the desert. The river usually refers to the mainstream from Xiaojiake to the Taitmar Lake with a length of 1.3×10^3 km. The region is suffering from extremely ecological degradation since 1970s. Nearly one-third chainage in the downstream of Tarim River has been dried out because of extensive agricultural exploration and improper irrigation methods. The drying of the lower reaches of the river has been accompanied by the drying and disappearance of the terminal lake (Lopnor lake) (Liu *et al.*, 2008). Ground-water levels have dropped to 5–8 m below the surface and the ground water has become salinized. The frequency of extreme weather conditions has increased (Song and Fan, 2000).

The Kaidu watershed is located in the middle reach of the Tarim River and has an area of approximately 19.0×10^3 km^2. Figure 3 shows the outline of the catchment with the major river system, rain gauges, and digital elevation model (DEM). There is no doubt that the discharge and flood events of Kaidu River not only represents destructive natural hazard in the mountainous, but also is the obvious complement for the lower reach of the Tarim River. The mean elevation of the watershed ranges from 2,400 to 2,600 m above sea level in the basin, and from 4,000 to 5,500 m in the mountain. The spatial and temporal distribution of precipitation is strongly heterogeneous. The average rainfall is about 273 mm/year. More than 80% of the total annual precipitation falls from May to September, and less than 20% of the total falls from November to the following April. The Kaidu watershed has an extreme cold climate with an average temperature of -4.16°C. Pan evaporation is about 1,157 mm/year. Snow melting is one of the main sources in spring. Snow and glacier are mainly distributed in the mutation area above 4,000–4,500 m. There are two possible water release peaks per year. The snow on the lower mountains melts in spring and glaciers in the high mountains melts in summer. Stream flow from May to October contributes more than 70% of the total flow. Peck flows at the Dashankou (DSK) station reach around 400–700 m^3 s^{-1} in August and September, and dropped to almost zero during the end of the dry season. The soils in Kaidu watershed consist of rock, loam, sand loam, slit clay loam, loamy sand, fine sand, and coarse sand. The land use is dominated by meadows (61%), followed by surface water bodies (20%), rocks (17.5%), and forests (1.5%).

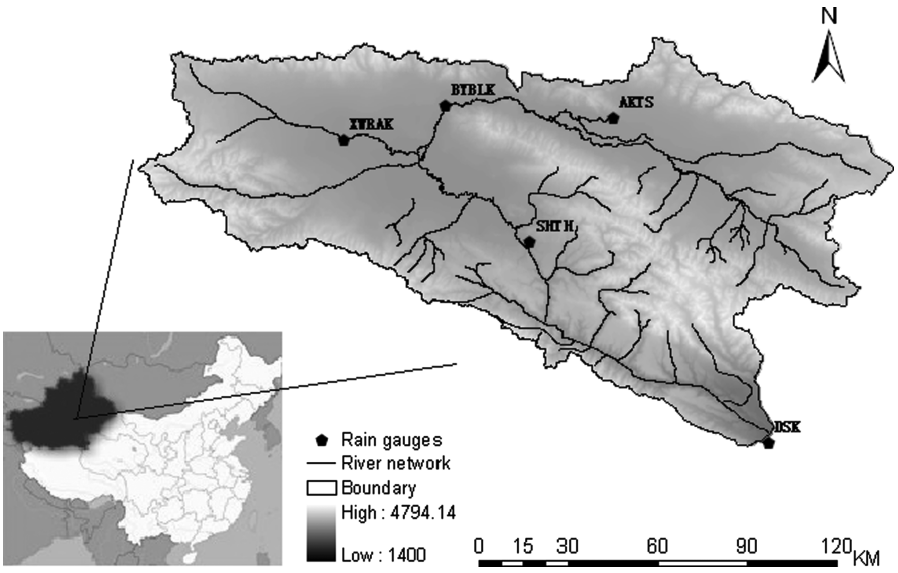

FIG. 3. Study system of Kaidu watershed.

Generally, the Tarim River Basin is a typical water-shortage area, with characteristics of low rainfall, high temperature, and high evaporation. The Kaidu River supplies water to the downstream region's municipal, industrial, and agricultural sectors and is also the most important source for ecosystem recovering of the lower reaches of the Tarim River. Conflict between economic development and ecological protection is increasingly serious. The intergrated modeling system could be used for simulating and managing water in more efficient and environmentally benign ways. Unfortunately, in the study watershed, there is a lack of effective tool for facilitating efficient, equitable, and sustainable water resources management. On the other hand, spatial and temporal variations exist in such system components as precipitation, evapotranspiration, snow melting, and stream flows. The water availability is directly dependent on the varying river flows. Currently, water resources management in the watershed is based mainly on statistical analyses of hydrologic data. Therefore, it is deemed necessary to develop effective modeling system for supporting water resources management in the study area under such complexities (Li and Huang, 2007).

Integrated modeling system

Figure 4 shows the framework of the integrated modeling system by coupling RS/GIS technique and distributed hydrological model. First, three sets of input data are collected (i.e., climate data from meteorological stations, land surface data derived from RS/GIS, and the climate parameters estimated by RS). Then, a distributed hydrological model of Kaidu watershed is set up with conventional gauges' data. The calibration and validation is performed for 4 years (1998–2001), and the stream flow of the rainy season in 2005 is also simulated. Another model is parameterized with the data of rainfall, PET, and LAI through the RS technique and is calibrated individually. Based on the two models with different setups, a comparison of simulation results is carried out. The horizontal model discretization is 5×5 km. Within each grid square, the vertical unsaturated soil profile is discredited into computational cells with typical sizes of 5–50 cm. Ground-water flow is described by interflow and base flow storages characterized by empirical time constants and threshold parameters. Climate, land surface, and soil parameters can be specified at each horizontal grid cell, and thus the spatial characteristics of the watershed can be taken into account.

Data availability

General meteorological data comprising air temperatures, pan evaporation, and daily rainfall are collected for the period of 1998–2001. Daily rainfall records are available from five

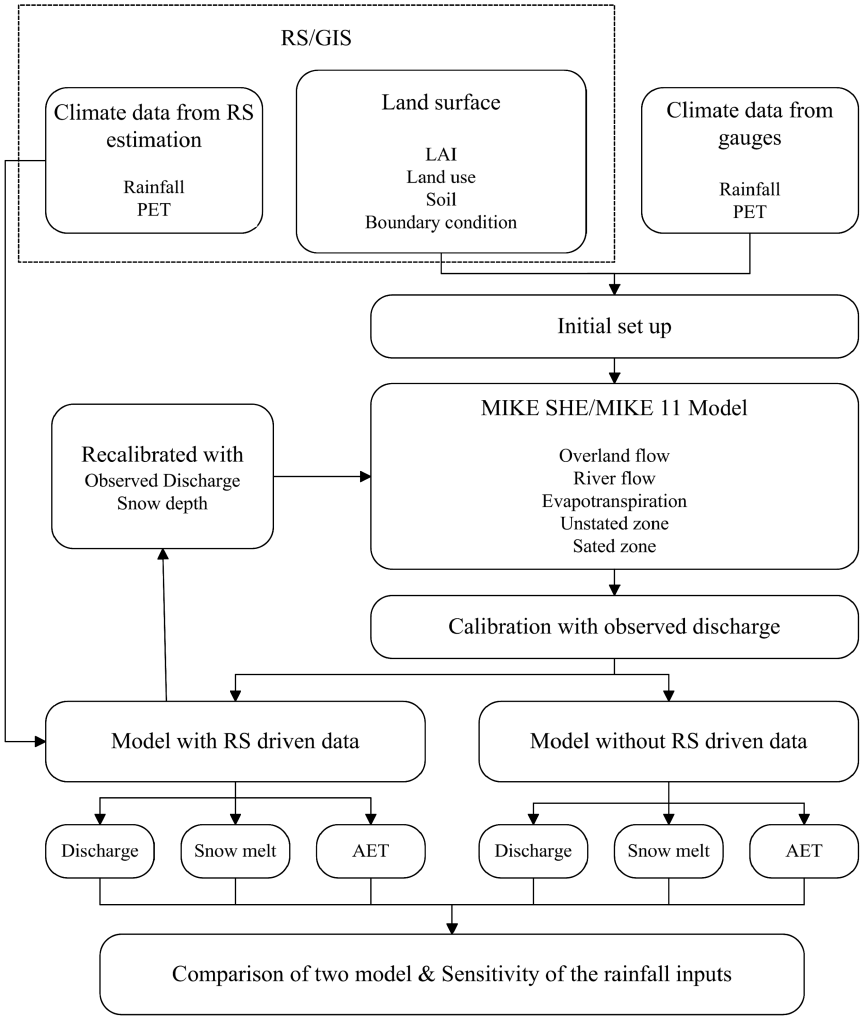

FIG. 4. Flow chart of the integrated modeling system for the Tarim River Basin management.

rain gauges within the Kaidu watershed and are used as inputs in each grid. It is spatially distributed according to Thiessen polygon technique. PET is estimated using the Penman–Monteith method and used as input to the model. These data are collected from a local institution of the Xinjiang Institute of Geography and Ecology (XIGE), located in Northwest China.

Four land cover types, namely meadows, forests, rocks, and surface water bodies, are identified in the Kaidu watershed for simulation purposes. The distribution of land cover is classified from the land cover coverage map in 2000, which was developed by the XIGE (Liu *et al.*, 2008). For each land cover type, a set of parameters including empirical constants used in the simulation of AET (C_1, C_2, C_{int}), time series for LAI, and RDF are entered in the MIKE SHE vegetation database. Most information is obtained indirectly from published reports and papers because no field data are available for each vegetation type. Values of C_{int}, C_1, and C_2 for each vegetation type are based on the research works of Vazquez and Feyen (2003). Values of LAI and RDF are obtained from the crop database of the MIKE SHE model (DHI, 2007). The soil map is obtained from the digital soil map processed by the XIGE. The soil in the watershed is divided into seven major types (i.e., rock, loam, sand loam, slit clay loam, loamy sand, fine sand, and coarse sand). The initial soil physical parameters for each soil type are derived from the DHI soil property reference (DHI, 2007). Geological property of the saturated zone is characterized by the horizontal hydraulic conductivity (K_H) and the vertical hydraulic conductivity (K_V). They are assumed to be linked by a constant anisotropy factor. Thus, only K_H is varied, while K_V is set equal to one-tenth of the respective K_H. The water exchange between river and saturated zone is accounted by a leakage coefficient (LC), which is assumed to be uniform in the model.

The input topography map is derived from the 90×90 m DEM processed by the XIGE. The river network and physical boundaries of the catchment are delineated from the DEM. RS-based LAI data are collected from the previous studies of Zhang (2006), whereas other RS-based parameters are processed by the Flemish Institute for Technological Research (VITO), Belgium. Table 1 presents the main input data and the associated sources.

Calibration and validation

Discharges are selected for calibration targets. Daily stream flow data from Bayinbuluk (BYBLK) and DSK gauging stations are used for calibration and validation. Nash-Sutcliffe coefficient (EF), water balance coefficient (RE), and correlation coefficient (R) are used to describe the quality of the simulation results (Vassiljev, 2006).

$$\text{Nash-Sutcliffe coefficient: } \mathrm{EF} = 1 - \frac{\sum_{i=1}^{n} (Q_{\mathrm{obs},i} - Q_{\mathrm{sim},i})^2}{\sum_{i=1}^{n} (Q_{\mathrm{obs},i} - \overline{Q}_{\mathrm{obs}})^2} \tag{21}$$

$$\text{Water balance coefficient: } \mathrm{RE} = 1 - \frac{\sum_{i=1}^{n} \left| Q_{\mathrm{obs},i} - Q_{\mathrm{sim},i} \right|}{\sum_{i=1}^{n} Q_{\mathrm{obs},i}} \tag{22}$$

Correlation coefficient:

$$\mathrm{R} = \frac{\sum_{t=1}^{T} (\mathrm{Q}_{\mathrm{obs,i}} - \overline{\mathrm{Q}}_{\mathrm{obs}})(\mathrm{Q}_{\mathrm{sim,i}} - \overline{\mathrm{Q}}_{\mathrm{sim}})}{\left[\sum_{t=1}^{T} (\mathrm{Q}_{\mathrm{obs,i}} - \overline{\mathrm{Q}}_{\mathrm{obs}})^2\right]^{1/2} \left[\sum_{t=1}^{T} (\mathrm{Q}_{\mathrm{sim,i}} - \overline{\mathrm{Q}}_{\mathrm{sim}})^2\right]^{1/2}} \tag{23}$$

where $Q_{obs,i}$ is the observed discharge at time step i, $Q_{sim,i}$ is the simulated discharge at time step i, $\overline{Q}_{obs}$ is the mean observed discharge and n is the total number of time steps (Nash and Sutcliffe, 1970). Note that the MIKE SHE estimations are optimal when EF, RE, and R are close to 1. With the calibrated parameters, validation is taken using daily discharge data in BYBLK and DSK stations. Additionally, the observed snow depth data at BYBLK station are compared with the simulated snow depth results.

Table 1. Date List of MIKE SHE Model

Parameter	*Source*	*Attribute*
(1) Distributed maps:		
Watershed boundary	Extract from DEM using GIS algorithms	1×1 km^2 grid
Topography	1:250,000 DEM	1×1 km^2 grid
Ditch network	Extract from DEM using GIS algorithms	1×1 km^2 grid
Soil type	Digital soil map of Kaidu Basin	Shapefile
Vegetation	Land sat TM-based land cover map	Shapefile
LAI	MODIS LAI data	1×1 km^2 grid
Root depth	Deduced from LAI variation	0–6 m
Precipitation zones	Stations distributed by Thiessen polygon method	1×1 km^2 grid
(2) Time series:		
Precipitation	Observed data from meteorological stations	5 stations
	FY_2C remote sensing data	5×5 km^2 grid
Potential evapotranspiration	Observed data of weather stations	2 stations
	MODIS estimation data	1×1 km^2 grid
Snow depth	Observed snow depth	1 station
Discharge	Observed data of hydrology stations	2 stations

DEM, digital elevation model; GIS, geography information system; LAI, leaf area index; TM, thematic mapper.

Table 2. Calibrated Value of Main Parameters for the Conventional Model

Parameter	*Calibrated value*
Manning coefficient of river ($m^{1/3}\ s^{-1}$)	33
Leakage coefficient (s^{-1})	0.1×10^{-6}
Vertical hydro conductivity of saturated zone ($m\ s^{-1}$)	0.29×10^{-3}
Horizontal hydraulic conductivity of saturated zone ($m\ s^{-1}$)	3.5×10^{-6}
Specific yield ($L^3/L^2/L$)	0.125
Manning coefficient of overland flow ($m^{1/3}\ s^{-1}$)	15

Results Analysis

Results with conventional data

Although data collection was conducted over a large number of years, complete and continuous stream flow data were identified within the period 1998–2001. The data were split into two parts (split-sample calibration-validation method), with calibration performed for the period January 1998 to December 1999 and validation for the period January 2000 to December 2001. The model could be updated when long time series of the meteorological and hydrological data are available.

Sensitivity analysis was conducted to investigate the effects of the model responses to its parameters and to identify those which should be further calibrated. The most sensitive parameters are vertical hydraulic conductivity of saturated zone (K_V), horizontal hydraulic conductivity of saturated zone (K_H), and manning coefficient of overland flow (M). Among these parameters, K_V has significant effect on the base flow. Larger K_V values could lead to higher cumulative infiltration through the soil surface (less runoff or overland flow) and could increase the ground-water level. Thus, higher K_V values could lead to lower and flatter peaks of stream flow. Lower K_V values could bring about an increased overland flow. The K_H could affect the base flows as well as the peak flows. Lower values could delay the flow reaching the stream. Higher values could result in draining the water more quickly and affect the base flow. M could affect the shape of overland flow, the peak value, and the relative importance of subsurface runoff to the overland flow. The higher the M value, the faster the water is routed overland toward the nearest river reach; thus peak runoff flows are particularly affected. Table 2 presents the final values of main parameters.

Figure 5a and b show the predicted and observed daily runoffs at the BYBLK and DSK stations during the calibration period. The correlation between these two sets of results is demonstrated in Table 3. The predicted data well matched the observed ones with the EF values of 0.79 at the outlet DSK station, and the RE and R values are 0.99 and 0.94, respectively. Model performances are lower at the BYBLK station with the EF, RE, and R values of 0.36, 0.70, and 0.77, respectively. Both in wet and dry seasons, river flows are overestimated with the maximum volume bias of 15%. Figure 5c and d show a comparison between the predicted and measured daily runoffs at the BYBLK and DSK stations

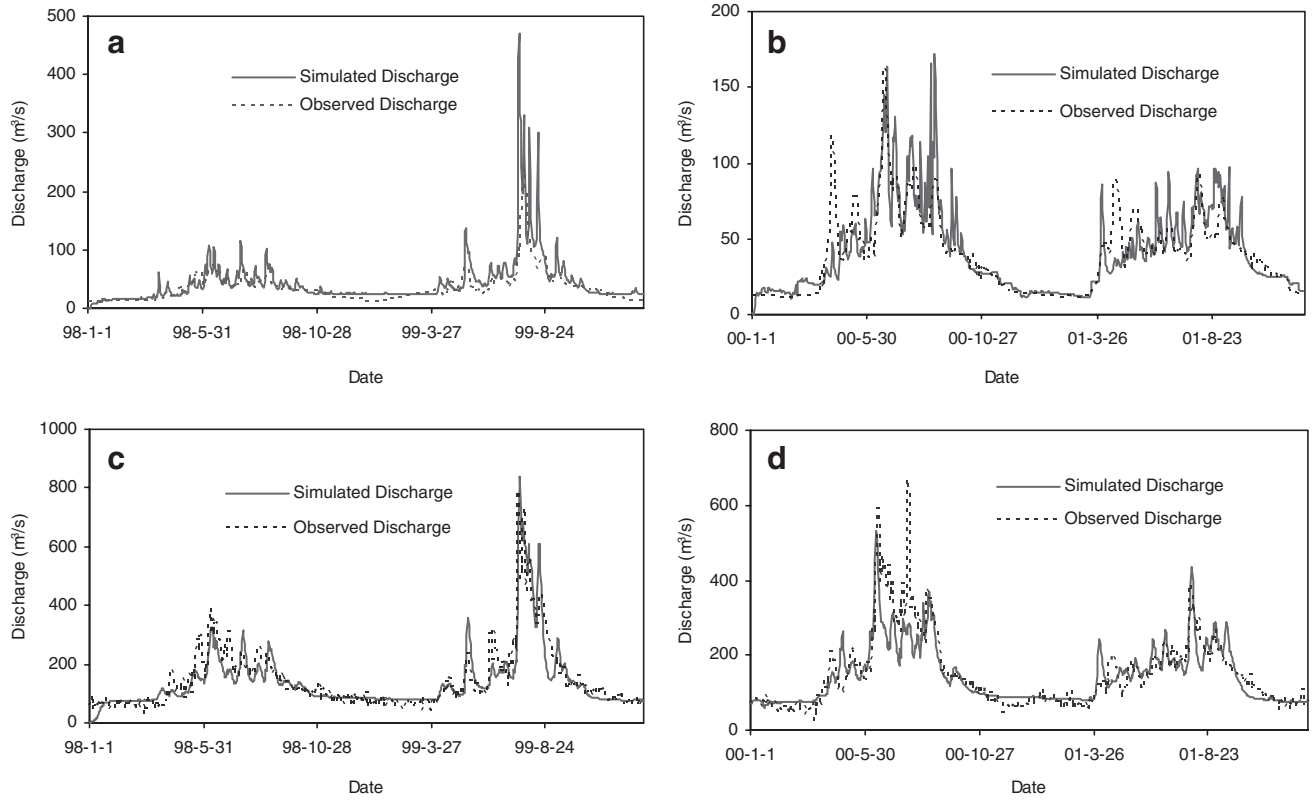

FIG. 5. Calibration and validation results of conventional model (1998–2001). (**a**) Calibration result of BYBLK station, (**b**) validation result of BYBLK station, (**c**) calibration result of DSK station, (**d**) validation result of DSK station. BYBLK, Bayinbuluk; DSK, Dashankou.

Table 3. Performance of Daily Runoff Simulation for the Conventional Model

	EF		*RE*		R	
Year	*BYBLK*	*DSK*	*BYBLK*	*DSK*	*BYBLK*	*DSK*
Calibration period	0.361	0.792	0.704	0.989	0.774	0.904
1998 spring	0.177	0.728	0.922	0.885	0.692	0.882
1998 summer	−2.80	−0.170	0.806	0.926	0.423	0.429
1998 dry season	0.170	−0.146	0.801	0.990	0.796	0.584
1999 spring	−1.533	0.267	0.688	0.946	0.721	0.656
1999 summer	−2.599	0.656	0.502	0.972	0.614	0.893
1999 dry season	−0.311	0.520	0.980	0.962	0.612	0.734
Validation period	0.319	0.720	0.833	0.979	0.702	0.849
2000 spring	−0.433	0.560	0.836	0.942	0.359	0.773
2000 summer	−1.125	0.183	0.985	0.809	0.430	0.692
2000 dry season	0.738	−0.084	0.942	0.990	0.870	0.487
2001 spring	−1.653	−0.65	0.974	0.888	0.633	0.368
2001 summer	−3.085	0.048	0.756	0.973	0.743	0.678
2001 dry season	0.276	0.390	0.959	0.961	0.631	0.702

EF, Nash-Sutcliffe coefficient; RE, water balance coefficient; *R*, correlation coefficient; BYBLK, Bayinbuluk; DSK, Dashankou.

during the validation period. The predicted runoff has significant correlation with the measured runoff. The *R*, RE, and EF for daily stream flow values are 0.72, 0.98, and 0.85 at the DSK station, and are 0.32, 0.83, and 0.70 at the BYBLK station, respectively. The timing and volume of the predicted peaks have a higher variance than the actual observation values. During the simulation of Kaidu watershed, the predicted dry season flow is underestimated about 28%, comparing with the measured flow. The wet season flow modeled is overestimated. The worst performance is in the dry season of 1998 with 92% volume bias.

To compare with RS-based model later, a reference run with the conventional data of rainy season in 2005 was conducted. Figure 6 shows that the predicted values match the observed ones well at the DSK outlet. The *R*, RE, and EF for daily stream flow values are 0.89, 0.967, and 0.68, respectively, for the simulation period.

Results from integrated modeling system

The RS-driven model was calibrated for the period of June to July (2005) and validated for the period of August to September (2005). When calibrating the RS-based model, the boundary conditions were well defined with zero inflow for both river and ground water. Table 4 shows the final values of hydrological parameters, which were assumed to be constant throughout the entire simulation period. Figure 7 shows the simulated and observed hydrographs for both calibration and validation periods. There was a statistically significant relationship between the predicted and the observed data, and the simulated river flow capture the interannual variations quite well. Table 5 presents the results at the outlet gauge. The simulation results are encouraging with EF ≥ 0.7.

In addition, a time series of simulated snow depth was extracted from the grid cell results of snow storage. The simulated snow depth was compared with measured values at the BYBLK test site for the rainy season 2005. Figure 8 shows a statistically significant relationship between the predicted and the observed data. The values of the EF and *R* are 0.49 and 0.63, respectively. The ranges of snow depth and the seasonal variation are matched.

Comparison of conventional and RS-based hydrological models

A comparison between the conventional hydrological model and the RS-based hydrological model was undertaken for the simulation period. The RS-based model was calibrated separately resulting in different optimized parameter sets. The most noticeable difference between two parameter sets is

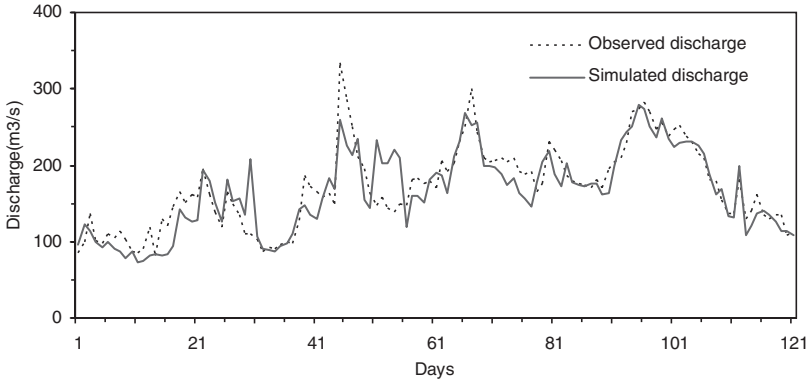

FIG. 6. Simulation results of conventional model (June to September 2005).

Table 4. Calibrated Value of Main Parameters of Remote Sensing–Based Model

Parameter	*Calibrated value*
Manning coefficient of river ($m^{1/3}\ s^{-1}$)	33
Leakage coefficient (s^{-1})	0.1×10^{-6}
Vertical hydro conductivity of saturated zone ($m\ s^{-1}$)	2.5×10^{-3}
Horizontal hydraulic conductivity of saturated zone ($m\ s^{-1}$)	3.5×10^{-6}
Specific yield ($L^3/L^2/L$)	0.125
Manning coefficient of overland flow ($m^{1/3}\ s^{-1}$)	15

in the parameter of K_V. The value is 2.5×10^{-3} in the RS-based model and 0.29×10^{-3} in the conventional model. Separate calibrations for the two models are necessary because of differences and bias in the rainfall, PET, and LAI inputs. Table 6 presents the statistics for model performance of the conventional and RS-based distributed hydrological models. Generally, the simulated stream flows are very similar to the two cases in both calibration and validation periods. The model with gauge-based inputs performs slightly better on water balance.

Because the spatial validation data are unavailable, the spatial patterns of the two models cannot be evaluated statistically. Instead, the comparisons of the simulated snow cover (SC) and AET of the two models are taken. Figure 9 shows the spatial distribution and the area comparison of the simulated SC during the period of 2005. The spatial distributions of the SC for both models are similar. The SC area simulated by the RS-based model are obviously larger than the conventional model results because of the overestimated rainfall inputs. However, the spatial pattern of simulated SC was not significantly influenced by the RS-based inputs.

Figure 10 shows the AET at the BYBLK station for the two sets of simulations, with the ranges of 0–6.5 mm/day for the conventional model and 0–8.3 mm/day for the RS-based model. Figure 11 shows that the spatial pattern of the simulated AET of the conventional model is clearly influenced by the precipitation zones, whereas the RS-based model outputs display a more gradual spatial variation. The average AET simulated by RS-based model is higher than the results of the conventional model. More smooth appearance outputs are caused by both the high spatial resolution of precipitation and PET inputs.

The use of RS-based inputs was expected to increase the spatial heterogeneity in the model simulations. The comparison between the conventional and the RS-based model shows that watershed responses might be similar on runoff generation and snow melting, but different in spatial pattern of AET. The potential advantage of the combination is that the RS-based hydrological model has better performances in the simulation of spatially distributed results. Generally, results from the RS-based model are more heterogeneous than the results from the conventional model (Stisen *et al*., 2008). In this study, the difference in the mean precipitation is, however, not transferred to the simulations of discharge because of individual calibration of the conventional and RS-driven

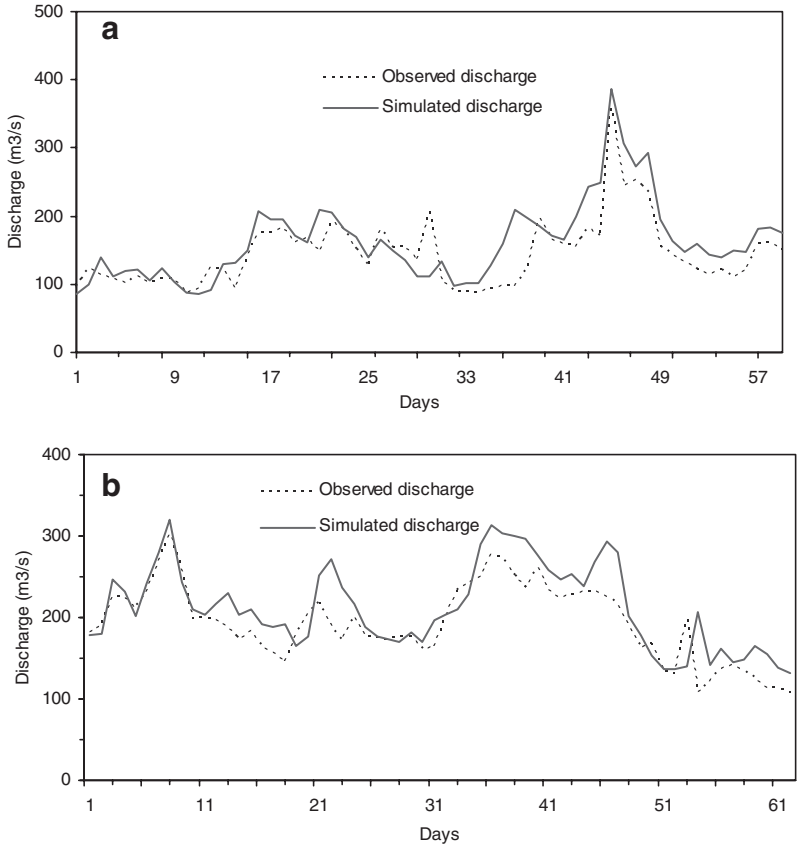

FIG. 7. Calibration and validation results of RS-based model. (**a**) Calibration period; (**b**) validation period. RS, remote sensing.

Table 5. Performance of Daily Runoff Simulation for Remote Sensing–Based Model

Year	*EF*	*RE*	R
Calibration period	0.708	0.953	0.915
Validation period	0.699	0.950	0.903

Table 6. Comparison of Performance of Remote Sensing–Based Model and Conventional Model

		Model performance		
Outlet gauge	*Input*	*EF*	*RE*	R
DSK	RS-based data	0.705	0.952	0.910
	Gauge-based data	0.686	0.967	0.890

RS, remote sensing.

models, but will consequently show up in the simulation results of AET.

Discussion

Because of low data availability, the rainfall inputs of the models are highly uncertain on temporal and spatial variabilities. Scenario simulation is used to quantify the effect of different rainfall inputs on simulation results. Figure 12 shows three rainfall input scenarios tested on the watershed: (a) single-gauge-based rainfall inputs: the observed records at the BYBLK meteorological station were selected; (b) gauges-based grid rainfall inputs: the observed records at five gauges were selected and distributed to the watershed by the Thiessen polygon method; (c) RS-based distributed rainfall inputs: the FY_2C rainfall products were selected. Figure 13 shows the characteristics of rainfall events. A statistically significant relationship exists between the RS-estimated monthly rainfall and the observed monthly rainfall. The *R*s are 0.944 at BYBLK station and 0.883 at DSK station (Fig. 13a). Comparing with the observation data, RS-estimated rainfall shows a considerably larger number of days with rainfall at BYBLK and DSK stations. The daily rainfall volumes of the observed data were dominated by small values, whereas RS-estimated rainfall have higher frequency of volume of >3 mm (Fig. 13b). In addition, the RS-estimated rainfall shows longer event duration, and the frequency of the event duration of ≥ 3 days is higher than the observed rainfall (Fig. 13c).

Figure 14 shows very similar performances for the three scenarios. The RS rainfall leads to slightly better performance, because more temporal and spatial information of the rainfall were captured by the FY_2C products. Table 7 presents that the scenario based on RS rainfall gets the best performance with an EF of 0.705, whereas the scenario based on uniform rainfall input gets the lowest EF value of 0.66.

In this study, the RS-based inputs seem to capture the rainfall variability and spatial pattern well, although only 9-month data are available. Compared with the gauge measurements, the volume of the RS-estimated rainfall is on average higher than the observed value. This is because all of the rain gauges are located below 3,000 m and the extreme single events at the high elevation cannot be captured by gauges. In addition, temporal variation of the rainfall inputs can also directly affect the stream flow results. Discharge of the stream flow increases with the event duration of the rainfall from the RS estimated. Even though the rain gauges can capture the volume variability well, it has difficulty in capturing the correct spatial pattern of rainfall. This might result in good runoff simulation but poor spatial representation within the watershed. The individual effect of the PET and LAI has not been examined, considering the lack of local calibration. There is no doubt that the rainfall inputs dominated the simulation of discharge, whereas rainfall, PET, and LAI will influence the volume and spatial patterns of AET. At short time scales during the rainy season, rainfall and PET are expected to dominate the AET simulations. At longer time scales, all three variables are, however, highly autocorrelated because of the tight relation between rain clouds, incoming radiation, and vegetation growth (Stisen *et al*., 2008).

Three important variables (i.e., precipitation, PET, and LAI) were derived from RS and used as drivers for the distributed hydrological model MIKE SHE; in this manner, the meteorological forcing is entirely based on products from satellite data. The satellite products may be subject to uncertainties and biases, which may lead to uncertain outputs of the hydrological model. Therefore, it is required to both validate the satellite products individually and access their predictive capability in the modeling framework, where their combined effect and inherent variability can be evaluated at catchment's scale. However, the RS-based data offer tremendous advantages, particularly in improving the spatial coverage of the meteorological input. Additionally, the RS data source have high temporal resolution (repetition time) to produce reliable daily estimates of precipitation and PET. Therefore, the RS data are essential input variables to most hydrological

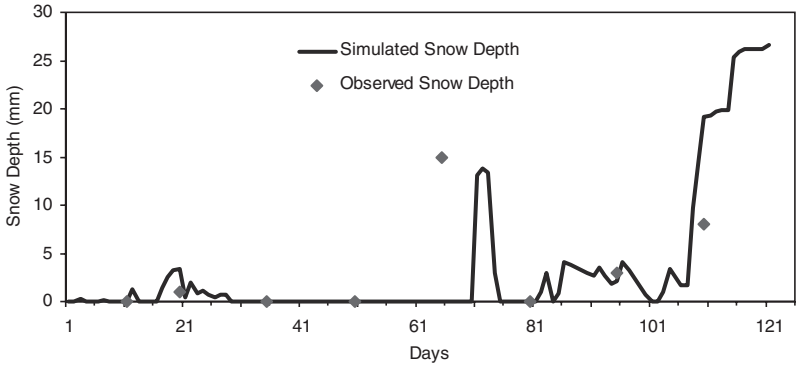

FIG. 8. Comparison of the simulated snow depth and observed snow depth at the BYBLK station.

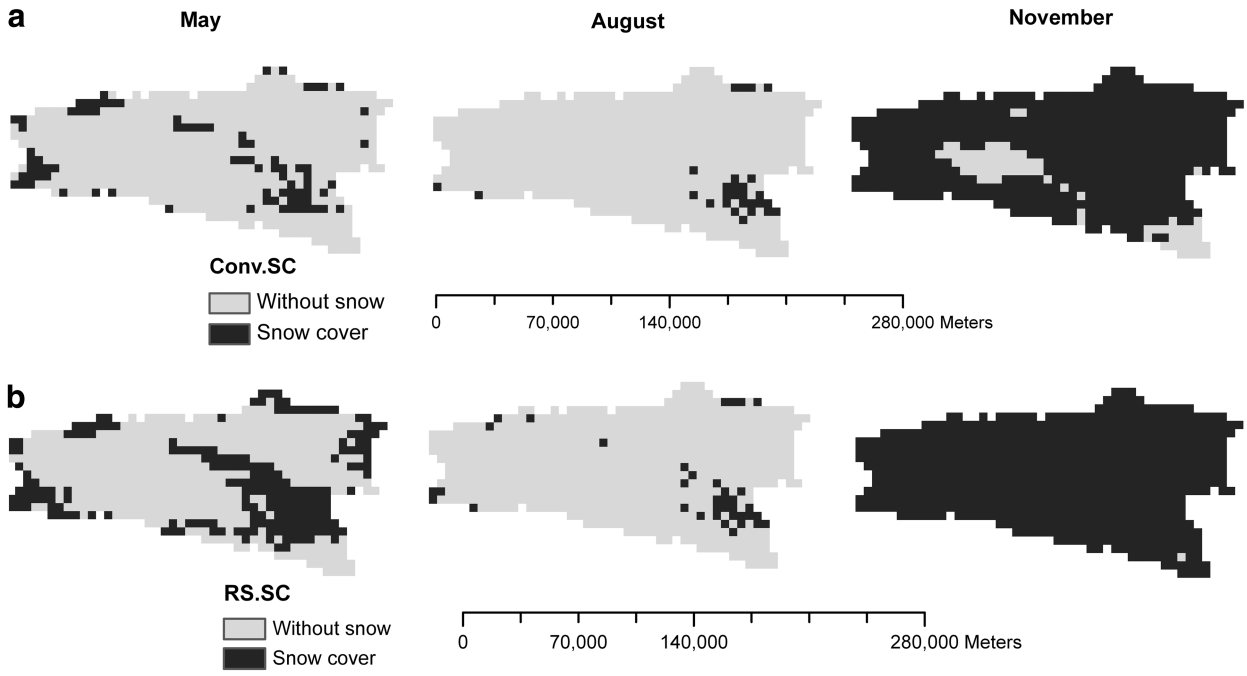

FIG. 9. Comparison of the simulated snow covers (SCs). (**a**) Simulated SC of conventional model; (**b**) simulated SC of RS-based model.

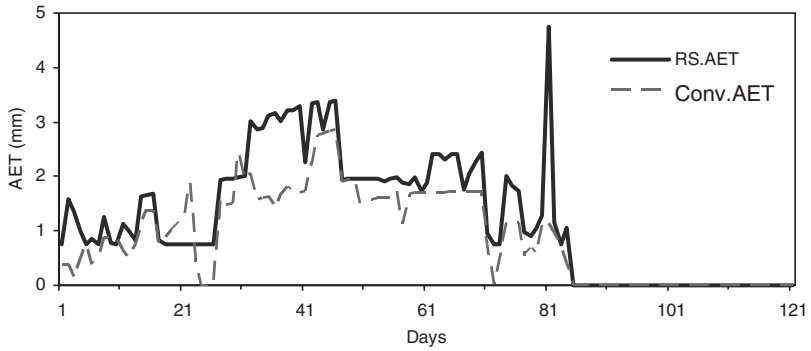

FIG. 10. Comparison of the simulated actual evapotranspiration (AET) at the BYBLK station.

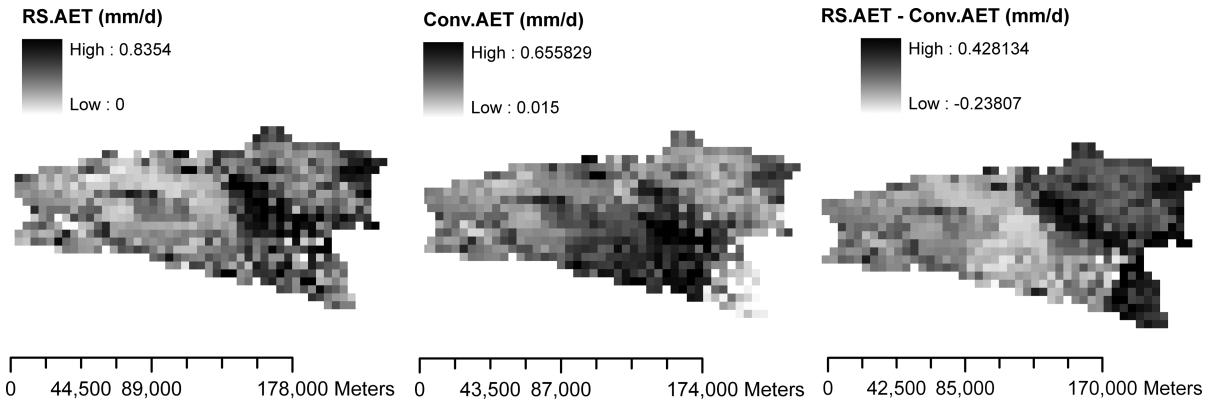

FIG. 11. Comparison of the average actual evapotranspiration (AET) of the rainy season in 2005.

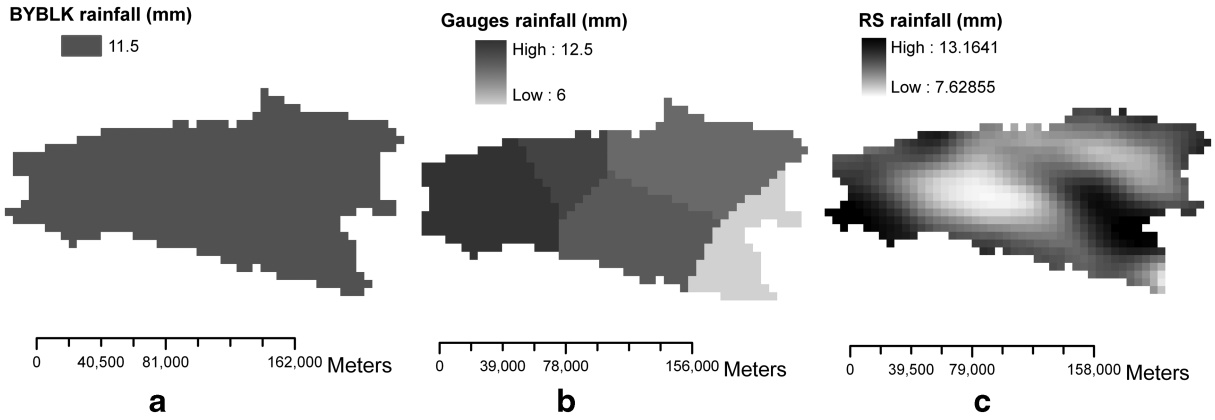

FIG. 12. Three rainfall inputs: (**a**) single-gauge-based rainfall inputs; (**b**) gauges-based grid rainfall inputs; (**c**) RS-based distributed rainfall inputs.

modeling studies concerning ground water, flooding, and integrated water management in many regions and countries where conventional meteorological data are sparse.

Previously, few studies for the Kaidu watershed showed that the lumped models could also simulate stream flows with high accuracy (Zhang, 2006). However, the lumped models assume the study watershed as a spatially homogeneous region, and the spatial heterogeneity of the climate variable and land surface cannot be considered (Bronster *et al.*, 2000). They are thus unable to predict SC, evapotranspiration, soil water content, and ground-water levels and are passive to the changes in land use, soil, and weather conditions. On the

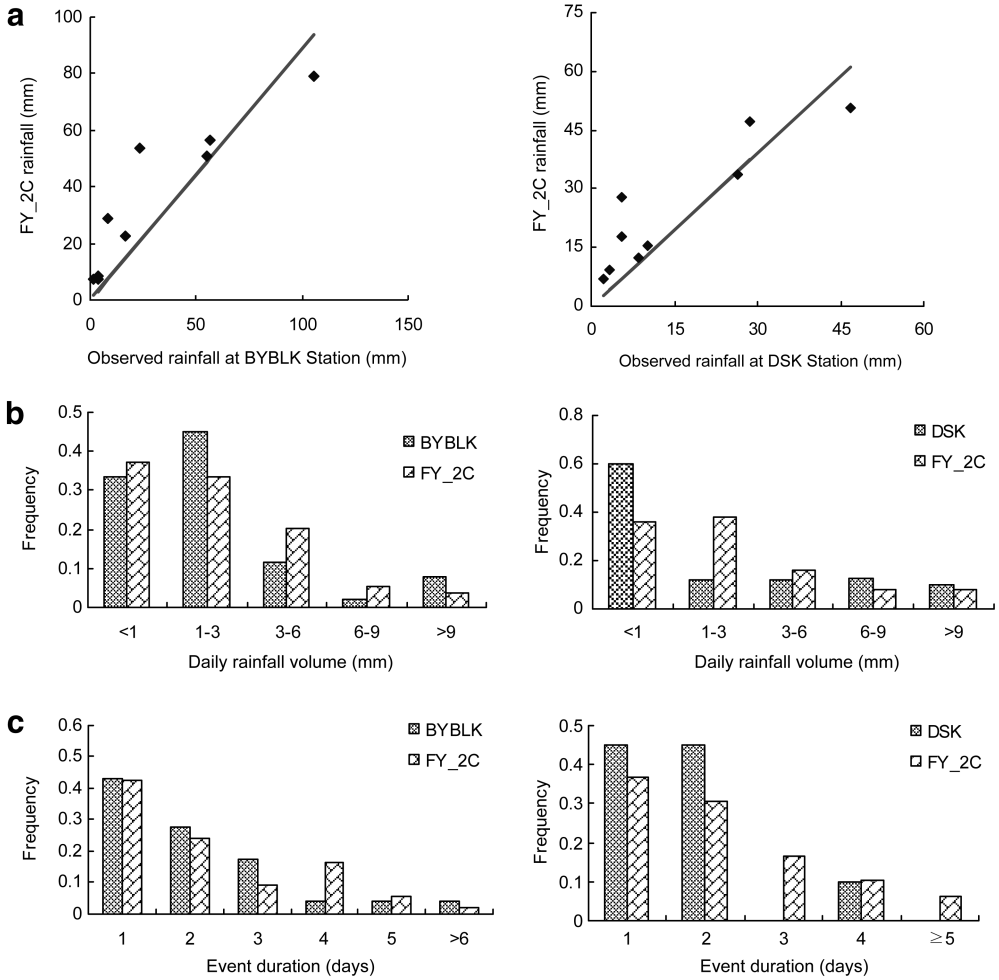

FIG. 13. Comparison of the RS-estimated rainfall and the observed rainfall. (**a**) Relationship between monthly rainfall volume; (**b**) average daily rainfall volume; (**c**) average duration of the events.

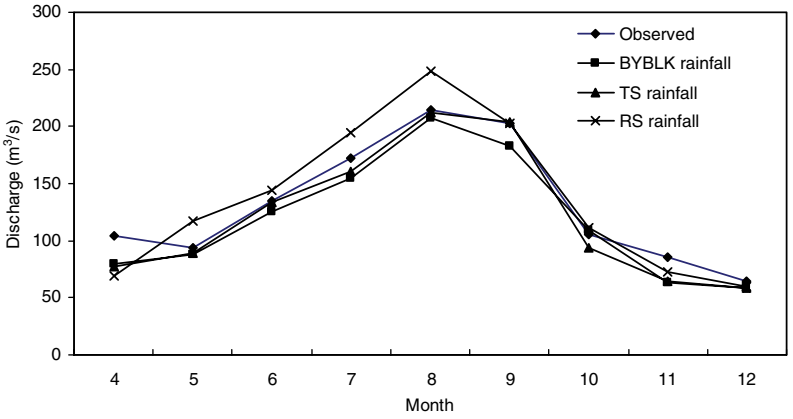

FIG. 14. Comparison of simulation results under different rainfall inputs.

other hand, the study area is a typical ungauged watershed where both conventional meteorological data and land surface data (i.e., land use, vegetation, and soil type) are sparse. There are high spatial and temporal variations existing in many system components, such as precipitation, evapotranspiration, snow melting, and stream flows. Thus, it is essential to develop a distributed hydrological model that could integrate RS data as inputs into the modeling framework. The results obtained show that MIKE SHE model can simulate the stream flows at all points in Kaidu watersheds with acceptable EF values. Similar results are presented in previous studies with the MIKE SHE model in such arid and semiarid watersheds (Andersen *et al.*, 2001; McMichael *et al.*, 2006).

Conclusions

In this study, an integrated modeling system has been developed for water resources management of the Tarim River Basin. The system is based on the RS/GIS technique and the distributed hydrological model. It can be useful for water resources management of many regions and countries where both rain gauges and field data are sparse. The developed modeling system has been used to simulate the stream flow, snow melting, and evapotranspiration of the Kaidu watershed. The modeling outputs are verified through available observation data, which have demonstrated reasonable prediction accuracy with $EF \geq 0.7$. Compared with the conventional hydrological model, the results indicate that the developed RS-based model has similar performance in runoff and snow melting simulations, whereas better performance in AET simulation. The results obtained can be used for helping planners to establish effective water exploitation and allocation policies and thus improve the local ecosystem sustainability.

The developed system was limited by the satellite data sources used, which have such short time series that could not be sufficient for describing the long-term variation of the study area. Currently, long time series of remotely sensed precipitation are unavailable. Consequently, future work can continue to focus on spatial calibration and validation of the modeling system. In addition, the satellite product inputs may be associated with many uncertainties and biases, which may limit their applicability in a real-world hydrological context. The model solution would be more applicable, if uncertainty analyses can be performed.

Table 7. Model Performance Under Different Rainfall Inputs

		Model performance		
Rain gauge	*Rainfall input*	*EF*	*RE*	R
DSK	FY_2C	0.705	0.955	0.933
	Single gauge	0.660	0.867	0.837
	5 gauges	0.693	0.953	0.866

Acknowledgments

This research was supported by the Natural Sciences Foundation of China (40730633 and 50979001). The authors are grateful to the editors and the anonymous reviewers for their insightful comments and suggestions.

Author Disclosure Statement

No competing financial interests exist.

References

Abbott, M.B., Bathurst, J.C., Cunge, J.A., Ocinnell, P.E., and Rasmussen, J. (1986). An introduction to the European hydrological system—systeme hydrologique Europeen, She. 2. Structure of a physically-based, distributed modeling system. *J. Hydrol.* 87, 61.

Andersen, J., Refsgaard, J.C., and Jensen, K.H. (2001). Distributed hydrological modelling of the Senegal River Basin—model construction and validation. *J. Hydrol.* 247, 200.

Apul, D., Gardner, K., and Eifhmy, T. (2005). Probabilistic modeling of one-dimensional water movement and leaching from highway embankments containing secondary materials. *Environ. Eng. Sci.* 22, 156.

Bastiaanssen, W.G.M., Menentia, M., Feddesb, R.A., and Holtslag, A.A.M. (1998). Remote sensing surface energy balance algorithm for land (SEBAL). *J. Hydrol.* 213, 198.

Bates, B.C., Kundzewicz, Z.W., Wu, S. and Palutikof, J.P. (2008): Climate Change and Water. *Technical Paper of the Intergovernmental Panel on Climate Change, IPCC Secretariat, Geneva.* 8.

Beven, K.J. (1979). On the generalized kinematic routing method. *Water Resour. Res.* 15, 1238.

Biftu, G.F., and Gan, T.Y. (2001). Semi-distributed, physically based, hydrologic modeling of the Paddle River Basin, Alberta, using remotely sensed data. *J. Hydrol.* 34, 137.

Bronster, A., Jaegr, A., Ciintner, A., Hauschild, M., Doll, P., and Krol, M. (2000). Integrated modeling of water availability and

water use in the semi-arid northeast of Brazil. *Phys. Chem. Earth B* 25, 227.

Burnash, R.J.C., Ferral, R.L., and Mcguire, R.A. (1973). *A Generalized Streamflow Simulation System: Conceptual Models for Digital Computers*. Sacramento, CA: Joint Federal-State River Forecast Center.

Crawford, N.H., and Linsey, R.K. (1966). Digital simulation in hydrology, Stanford Watershed Model IV. Technical Report 39, Department of Civil Engineering, Stanford University, California.

Danish Hydraulic Institute (DHI). (1999). *MIKE SHE Water Movement: User Manual*. Hørsholm, Denmark.

Danish Hydraulic Institute (DHI). (2007). *MIKE 11 User's and Reference Manual*. Horsholm, Denmark: DHI Water & Environment.

Deng, M.J. (2006). Changes of climate and runoff in Tarim River Basin and ecosystem restoration in the lower reaches of Tarim River. *J. Glaciol. Necrol.* 28, 694.

Grayson, R.B., Moore, I.D., and Mchahon, T.A. (1992). Physically based hydrological modeling. 1. A terrain-based model for investigative purpose. *Water Resour. Res.* 28, 2639.

Grimes, D.I.F., and Diop, M. (2003). Satellite-based rainfall estimation for river flow forecasting in Africa. I: rainfall estimates and hydrological forecasts. *Hydrol. Sci. J.* 48, 567.

Jakeman, A.J., Litlewood, I.G., and Whitehead, P.G. (1990). Computation of the instantaneous unit hydrograph and identifiable component flows with application to two small upland catchments. *J. Hydrol.* 117, 275.

Kristensen, K.J., and Jensen, S.E. (1975). A model for estimation the actual evapotranspiration from the potential one. *Nord. Hydrol.* 6, 170.

Li, Y.P., and Huang, G.H. (2007). Inexact multistage stochastic quadratic programming method for planning water resources systems under uncertainty. *Environ. Eng. Sci.* 24, 1361.

Li, Y.P., Huang, G.H., and Nie, S.L. (2006). An interval-parameter multistage stochastic programming model for water resources management under uncertainty. *Adv. Water Resour.* 29, 776.

Li, Y.P., Huang, G.H., Yang, Z.F., and Nie, S.L. (2008). Interval-fuzzy multistage programming for water resources management under uncertainty. *Resour. Conserv. Recycl.* 52, 800.

Liu, H.L., Chen, X., Bao, A.M., and Wang, L. (2008). Investigation of groundwater response to overland flow and topography using a coupled MIKE SHE/MIKE 11 modeling system for an arid watershed. *J. Hydrol.* 347, 448.

Ma, J.Z., Wang, X.S., and Edmunds, W.M. (2005). The characteristics of ground-water resources and their changes under the impacts of human activity in the arid Northwest China-a case study of the Shiyang River Basin. *J. Arid Environ.* 61, 277.

McMichael, C.E., Hope, A.S., and Loaiciga, H.A. (2006). Distributed hydrological modelling in California semi-arid shrublands: MIKE SHE model calibration and uncertainty estimation. *J. Hydrol.* 317, 307.

Nash, J.E., and Sutcliffe, J.V. (1970). River flow forecasting through conceptual models part1—a discussion of principles. *J. Hydrol.* 10, 282.

Ouyang, R.L., Cheng, W.M., Wang, W.S., Jiang, Y., Zhang, Y.C., Wang, Y.Q. (2007). Research on runoff forecast approaches to the Aksu River basin. *Sci. China D Earth Sci.* 50(Supp. I), 16.

Refsgaard, J.C. (1997). Parameterisation, calibration and validation of distributed hydrological models. *J. Hydrol.* 198, 69.

Sahoo, G.B., Ray, C., De Carlo, E.H. (2006). Calibration and validation of a physically distributed hydrological model, MIKE SHE, to predict stream flow at high frequency in a flashy mountainous Hawaii stream. *J. Hydrol.* 327, 94.

Song, Y.D., and Fan, Z.L. (2000). *Resources and ecology of Tarim River, China*. Ulumuq: People Press of Xinjiang.

Stisen, S., Jensen, K.H., Sandholt, I., and Grimes, D.I.F. (2008). A remote sensing driven distributed hydrological model of the Senegal River basin. *J. Hydrol.* 354, 131.

Su, Z. (2002). The surface energy balance system (SEBS) for estimation of turbulent heat fluxes. *Hydrol. Earth Syst. Sci.* 6, 85.

Vassiljev, A. (2006). Comparison of two one-dimensional nitrogen leaching models at the watershed scale. *Environ. Eng. Sci.* 23, 225.

Wu, S.F. (2003). The change of river runoff during recent 30 years in Xinjiang. *Arid Land Geogr.* 25, 708.

Xu, H.L., Ye, M., and Song, Y.D. (2007). Relationship between climate changes and annual runoff of headstream s of Tarim River. *Sci. Geogr. Sin.* 2, 219.

Zhang, Y.C. (2006). A study on hydrological process response to environmental change in Kaidu watershed. PhD Thesis of Graduate School, Chinese Academy of Sciences. 53.

Zhang, Y.C., Li, B.L., and Cheng, W.M. (2004). Hydrological response of runoff to climate variation in Kaidu catchment. *Resour. Sci.* 26, 69.

Zhao, C.S., Shen, B., Huang, L.M., Lei, Z.D., Hu, H.P., Yang, S.X. (2009). A dissipative hydrological model for the Hotan Oasis (DHMHO). *Water Resour. Manag.* 23, 1183.